Article

The Application of Finite Element Simulation and 3D Printing in Structural Design within Construction Industry 4.0

Faham Tahmasebinia [1,*] , Amir Abbas Jabbari [1] and Krzysztof Skrzypkowski [2,*]

1   School of Civil Engineering, The University of Sydney, Darlington, NSW 2008, Australia
2   Faculty of Civil Engineering and Resource Management, AGH University of Science and Technology, Mickiewicza 30 Av., 30-059 Krakow, Poland
*   Correspondence: faham.tahmasebinia@sydney.edu.au (F.T.); skrzypko@agh.edu.pl (K.S.)

Abstract: Three-dimensional (3D) printing, or additive manufacturing (AM), is a production can be utilised to fabricate 3D shapes from a simulated file. This technology has gained global popularity in the construction industry since 2014 due to its wide range of applications. AM promotes a more automated, innovative, flexible, and sustainable construction method, making it an integral part of the Construction Industry 4.0. However, there need to be more detailed studies regarding the effectiveness of AM as the future direction in the construction industry. This paper investigates the application of the finite element method (FEM) in assessing 3D-printed structures to get insight into the performance of these structures. Three leading 3D-printed structures were selected, including Dubai Future Foundation in the United Arab Emirates, Apis Cor house in Russia and PERI house in Germany. Structural and thermal analyses, including linear static, natural frequency, spectral response, and steady state heat, were performed using Strand7 to assess the effectiveness of AM in construction and the reliability of FEM in analysing 3D-printed structures. Although there are limited standards and regulations for 3D-printed structures in most countries, it was concluded that 3D-printed structures presented a similar strength to traditional ones. Moreover, FEM can be used to provide a reasonable analysis of the performance of these structures, while complying with the relevant standards. This paper presents a novel numerical procedure to assess the performance of small-scale 3D-printed structures under various mechanical and thermal loadings by checking against the relevant standards.

Keywords: finite element modelling; 3D printing; Design and Analysis; Construction Industry

1. Introduction

1.1. Overview

Three-dimensional (3D) printing, or additive manufacturing (AM), is a technology used to manufacture 3D objects from a digital file. The American Society of Testing and Materials (ASTM) defines AM as "a process of joining materials to make objects from 3D model data, usually layer upon layer, as opposed to subtractive manufacturing methodologies" [1].

The first 3D printer was developed in 1984 by Chuck Hull, as a complex and expensive technology for prototyping with few applications. However, due to technological advancements, 3D printers can manufacture complex objects with increased applications in various industries, such as construction. Moreover, the automated, innovative, flexible, and sustainable nature of 3D printing has turned AM into a promising technology in Construction Industry 4.0 [2].

1.2. Problem Significance and Definition

The globalisation and the standardisation of 3D printing can significantly impact sustainable development goals (SDGs). SDGs are a collection of 17 interlinked global goals

to end poverty, protect the planet and ensure the global well-being of human beings by 2030 [3]. Hence, the adaption of AM in construction can contribute to the SDGs.

In addition, 3D printing provides constructability and sustainability benefits, leading to a faster, safer, cheaper, and more sustainable construction method.

Awareness of 3D printing in construction is proliferating. According to Google Trend [4], the search query "3D printing in construction" has reached multiple breakouts since 2014, showing the popularity of AM over the past decade. However, there are limited construction regulations set in most countries regarding the use of 3D printers. This is mainly due to the immaturity of AM in construction and limited research around the performance of 3D-printed structures.

The finite element method (FEM) has a wide range of applications in structural analysis and is used to assess the performance of 3D-printed structures. One of the benefits of FEM is its high accuracy due to the fine discretisation of the elements [5]. As a result, FEM has been deemed a reliable numerical method in structural analysis [6] and was used in this paper to analyse three 3D-printed structures.

2. Literature Review

This section aims to conduct state-of-the-art research on the problem definition. Therefore, a chronological and topical order was used to investigate the application of AM and FEM as a future direction in Construction Industry 4.0.

2.1. Construction Industry 4.0

The fourth revolution in the construction industry, known as Construction Industry 4.0, promotes more innovative, digitalised, integrated and automated construction processes [7]. There are six main steps to creating a framework for successfully implementing Construction Industry 4.0, as shown in Figure 1.
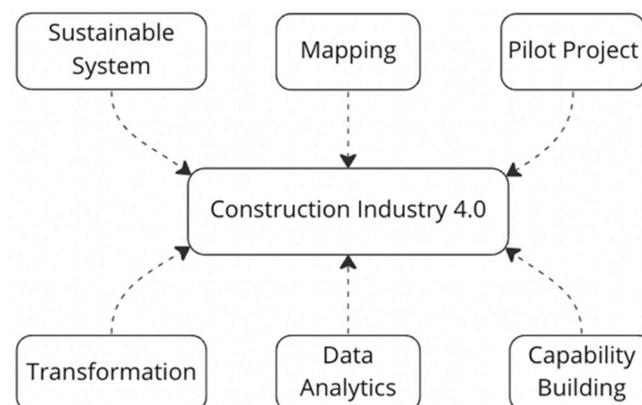

Figure 1. Implementation framework of Construction Industry 4.0.

The first step is mapping. Mapping aims to outline the digital maturity within the construction industry and sets targets for the future direction. As a result, mapping focuses on digitalisation in construction, including building information modelling (BIM) BIM-based project management [8,9] automation [10], supply chain [11] and document management [12]. The second step is pilot projects. Pilot projects are designed as proof of concept and allow digital leaders to apply innovation and digitalisation in the construction industry. Therefore, this step aims to collaborate with digital leaders to validate the end-to-end concept of Construction Industry 4.0 [13]. The third step is building capability. This step aims to develop pilot projects by incorporating robot usage [14] and digital fabrication [10], such as 3D printing. This highlights additive manufacturing as a significant contributor to Construction Industry 4.0. The fourth step is data analytics. This step integrates managerial and stakeholder objectives and BIM data using machine learning and artificial intelligence [15]. The fifth step is the transformation of digital en-

terprises within the industry. This focuses on emerging technologies [16] and removing obstacles [17]. The sixth step is a sustainable system that promotes the importance of having a sustainable system that addresses supply chain continuity challenges. Therefore, this step focuses on setting new policies and regulations [15] and the use of sustainable technologies, including AM.

2.2. Background on 3D Printing

The first 3D printer was developed by Chuck Hull in 1984, as an AM technology with limited application. Due to technological advancements, 3D printing has become a popular technology with various applications in multiple industries, including construction [18].

The increased popularity of 3D printing in the construction industry led to the serial production of 3D printers in 2015. Moreover, the emergence of building information modelling (BIM) enhanced the capability of AM [19] by creating a holistic process of creating and managing information for a built asset [20]. This makes AM and BIM an integral part of Construction Industry 4.0.

2.3. Principles of 3D Printing

The 3D printing technology relies on the fundamental principle of reducing the 3D volume into a sequence of 2D layers [21]. This process uses a BIM software, such as Autodesk Revit 2022 [22], to apply this principle using various additive technologies.

Stereolithography (SAL) is a standard additive technology to produce 2D layers, using a photochemical process. This process uses a high-powered laser that triggers a reaction in monomers and oligomers in resin. This reaction forms a polymer and hardens the resin to create 3D objects [23]. Selective laser sintering (SLS) is another additive technique that uses a powerful laser in joints, defined by the BIM software and hardens the powdered materials into solid 3D objects [1]. Fused filament fabrication (FFF) uses the extrusion technique to deposit building materials through a heated nozzle by establishing the object's outline and filling the enclosed area [24]. One of the benefits of FFF is the flexibility of building materials. FFF can use a wide range of filaments, including wax, plastic, ceramic, and concrete [21]. Moreover, the nozzle size can be adjusted based on the objects and filaments [25]. Therefore, FFF has become a popular additive technique in construction and is widely used in construction 3D printers.

2.4. Three-Dimensional (3D) Printing Materials in Construction

Three of the most used printing materials in construction are cementitious, polymer and metallic materials [24]. These materials are deposited into layers using the FFF technique. One of the printing material limitations is incompatibility with concrete reinforcement, which can be addressed using a fibre-reinforced concrete composite (FRC) [26]. FRC can improve the flexural strength of concrete to a value similar to reinforced concrete members [27].

2.5. Benefits of 3D Printing in Construction

The benefits of 3D printing can be categorised into two groups: constructability and sustainability [21].

2.5.1. Constructability Benefits

AM can lead to faster construction than traditional methods [22]. For example, using 3D printing to create a wall reduced the construction time from 100 to 65 h [28]. Moreover, faster construction results in faster commissioning, leading to mass production.

Using 3D printing can dramatically reduce the cost throughout the project. Due to storing capability of 3D printing, the cost of storage and transporting materials can be reduced [2]. Moreover, since the 3D printer only requires one operator, labour costs can also be reduced. For example, the application of 3D printing resulted in a 60% lower labour cost in constructing the Dubai Future Foundation (DFF) [29].

Flexible design and freedom in construction have made 3D printing a promising technology among engineers and architects. As opposed to the traditional and expensive construction methods, AM can build the structure of various complex geometries [30]. This promotes freedom in structural design and can lead to innovative designs by architects [31].

The supply chain is considered a time-consuming, yet critical, part of every construction project that can be shortened using 3D printing. By printing on demand using raw materials, the lead time of materials will reduce dramatically [32]. In addition, due to automation, AM reduces human intervention, leading to a shorter and more efficient supply chain system [33].

2.5.2. Sustainability Benefits

One of the primary benefits of 3D printing in construction is its contribution to the Sustainable Development Goals (SDGs), as summarised in Table 1.

Table 1. Contribution of 3D printing to Sustainable Development Goals (SDGs).

Sustainable Development Goal (SDG)	Description
SDG 1	No poverty
SDG 9	Sustainable cities and communities
SDG 12	Responsible consumption and production
SDG 13	Climate action

The adaption of 3D printing could contribute to no poverty (SDG 1), as it significantly reduces construction and labour costs leading to more affordable housing [34]. Moreover, unlike traditional construction methods, 3D printing is innovative, automated and sustainable [2], aligning with SDG 9 and SDG 11. Compared to the reductive manufacturing, additive manufacturing uses a closed-loop process, leading to significantly less waste during production, contributing to SDG 12 and SDG 13 [34].

AM in construction is considered sustainable and eco-friendly [22]. Moreover, construction 3D printers can use recyclable filaments, such as concrete mixed with recyclable materials. In addition, 3D printing builds by establishing the object's outline and filling the enclosed area [24]. Therefore, construction waste is estimated to reduce by 30–60% [35].

Another sustainable benefit of 3D printing in construction is reduced framework. The frameworks used for concrete are mainly made from wood, resulting in using trees. Since 3D printing is on-site, the need for wooden form and environmental impact reduces significantly [32].

Three-dimensional printing can also result in a safer working site. Safety is a significant challenge in the construction industry. Since 3D printing is automated and requires minimal human intervention, it could reduce the work hazard and promote safer construction sites [32].

2.6. Challenges of 3D Printing in Construction

As a new technology, 3D printing has several drawbacks. These drawbacks can be grouped into five categories: challenges with materials, 3D printers, architecture, construction management and regulations [21].

Printability, buildability and open time are some of the challenges with the material. Printability is the process of pumping and printing materials, such as concrete [36].

For the sake of enhancing printability, materials should have the right consistency for the nozzle, limiting the use of reinforced bars, unlike traditional construction materials [26]. Obtaining this condition, materials should be workable and include the right mixture of content [37]. Moreover, deposited printing materials should be able to resist deformation subjected to different loadings. This phenomenon is known as buildability [36]. Consistency between buildability and printability is one of the significant factors during construction.

Some of the 3D printer-related challenges are scalability and directional dependency. Traditionally, 3D printers were able to create objects strictly smaller than the chamber

volume of the 3D printer. This situation can be challenging for large-scale construction projects [38]. In addition, additive manufacturing uses a filament which could impact material load-bearing capacity and strength properties [39]. This setting is due to the directional dependency used in layered manufacturing.

Another challenge of 3D printing is related to architecture and structural integrity. Most BIM software excludes building services such as electrical and plumbing. Therefore, an additional reductive effort is needed to account for services. This can affect the structural integrity of the building and could lead to structural defects [30].

Using 3D printing can also challenge construction management. Since additive manufacturing is a new technology in construction, it could be challenging to provide accurate cost estimation and scheduling [21]. Moreover, 3D printing requires a complex installation and controlled environment, making it a challenging technology.

One of the substantial challenges of 3D printing is the need for design codes and regulations. A clear legitimate framework is required to affect the adaption of 3D printing in construction. Moreover, developing reliable numerical design methods can lead to overcoming liability issues for construction companies [35].

2.7. Future Direction of 3D Printing in Construction

The effort to use 3D printing as a sustainable construction method is growing. According to the Construction Industry 4.0 framework, discussed in Section 2.1, the successful implementation of 3D printing requires global awareness and regulations [15]. Given the benefits of AM and its alignment with SDGs, it can be expected to see more countries setting regulations across the use of 3D printing in construction.

In addition, due to advancements in technology, the adaption of AM could lead to more innovative construction methods. An example of this would be the use of cable frames to address the scalability challenges and introduce new alternative materials instead of steel-reinforced concrete, such as fibre-reinforced concrete composites (FRCs) [26].

2.8. Finite Element Method (FEM) and 3D Printing

The Finite Element Method (FEM) is a standard method for numerically analysing structures. Since FEM uses the discretisation of the structure into small elements, it is deemed an accurate and reliable method for structural analysis [6].

FEM can also be used to assess the accuracy of 3D-printed buildings. This helps analyse the performance of a proposed 3D-printed structure prior to its construction. In one study, it was observed that FEM could give an accurate quantitative estimation of unconfined uniaxial compression tests (UUCT) and direct shear tests (DST) of a 3D-printed building [40]. Since the numerical and experimental results were consistent, FEM could be a viable method for analysing 3D-printed structures.

2.9. Reliability and Constraints of FEM

FEM is a reliable numerical method of analysis due to discretisation. Using discretisation, the structure is subdivided into smaller elements connected with nodes. Each element is called a finite element, which has the same behaviour as the whole structure and is analysed using a discrete system of equations. It is then integrated through the whole system to approximate its behaviour [41].

One of the constraints of FEM is associated with the meshing process. Meshing is the process of discretising the structure into smaller defined elements. This process controls the accuracy of the analysis and is based on engineering judgement. Generally, finer meshing results in more accurate results; however, it also increases the computational time and cost [41]. Reasonable effort was made in preparation for this paper to minimise the inaccuracy caused by meshing.

3. Method

3.1. Tools and Software

Strand7 was used as the leading software in this paper. Strand7 Release 3 (R3) is a finite element analysis (FEA) software developed in Australia that provides an all-in-one solution to complex engineering problems. Table 2 summarises some of the benefits [42] and limitations of Strand7.

Table 2. Benefits and limitations of Strand7.

Benefits	Comprehensive library for material properties based on the standards
	Integrated modelling and analysis functionality within the software
	Extensive range of solvers and industry-standard libraries
Limitations	Outdated user interface and initial learning curve for new users
	Limited modelling options compared to AutoCAD

In addition to Strand7, Google Maps and Google Earth were used to get basic geometries of the structures of which the dimensions were not publicly published.

The effectiveness of three 3D-printed structures was investigated in this paper. These structures are the Dubai Future Foundation in the United Arab Emirates (UAE), Apis Cor house in Russia and PERI house in Germany.

3.2. Overview of the Structures

3.2.1. Dubai Future Foundation in UAE

Dubai Future Foundation (DFF) was built in the city of Dubai in 2016 and is known as the first 3D-printed concrete office in the world. DFF has a total office area of approximately 185 square meters, consisting of four cassettes. Each cassette comprises two U-shaped sections with a maximum length, height, and width of 8.1 m, 2.1 m and 2.1 m, respectively. The substructure was printed using a 6 m tall 3D printer capable of printing concrete layers, with a maximum width and thickness of 50 mm and 20 mm, respectively.

A truss system was formed along the entire perimeter of the cassette to increase the resistance of each cassette to vertical and lateral loads. In addition, longitudinal post-tensioning (PT) was used to enhance the bending resistance by passing post-tensioned steel bars through the voids and filling them with grout.

It was observed that the 3D printer was incapable of printing concrete with high tensile strength, which resulted in low-tensile concrete, with a tensile strength of about 10% of its compression strength. To address this limitation, steel reinforcements were added manually between the layers to increase the flexural stiffness of the structure.

3.2.2. Apis Cor House in Russia

Apis Cor House (ACH) is the first 3D-printed residential house in Russia, which was printed in less than 24 h. The ACH total area of 37 square meters was built entirely on-site using a crane 3D printer. Moreover, a complex geometry was adapted to showcase the capabilities of 3D printers.

The construction began by extruding the concrete paste to form the interior and exterior of the walls. After, steel reinforcement bars were placed between the voids and filled with grout [43].

According to Arch20, two main challenges were faced during the construction of ACH. Using a flat roof made it challenging to resist the snow load effectively. This was addressed by using polymer concrete for printing the roof system. The construction of ACH was initiated in the severe winter of Russia, which made it challenging to meet the ideal working temperature. Although the 3D printer could work at temperatures down to $-35\ ^\circ$C, it was required to have a site temperature of at least 5 $^\circ$C for the concrete paste. Therefore, it was proposed to isolate the site using a tent.

ACH is an excellent example of the application of 3D printing for the mass construction of affordable housing. This leads to sustainable cities and communities, contributing to SDG 9, as discussed in Section 2.5.2. In addition, the total cost of ACH was about AUD 16,500, equating to AUD 440 per square meter. This resulted in a total saving of 70% of the construction cost [43].

3.2.3. PERI House in Germany

The PERI house (PERIH) is the first 3D-printed residential house in Germany. It consists of two levels, each with an area of 80 square meters, resulting in a total area of 160 square meters.

PERIH was printed using a BOD2 printer capable of printing 1 m of concrete per second, making it the fastest concrete printer on the market. Unlike the crane printer used in ACH, the BOD2 printer uses a solid metallic frame, enabling the printer to travel in any direction along the three axes. One of the advantages of the BOD2 was the consideration of building services, such as pipes, electricity, and other utilities. This reduced the project's slack time and enabled the engineers to work on the building during the printing process [44].

The construction of PERIH followed the same process as outlined for ACH in Section 3.2.2. However, PERIH used an extra layer of insulation for each wall. Moreover, the construction of PERIH highlighted the future potential of 3D printing in the construction industry and initiated regulations in Germany [44].

This paper analysed the performance of the mentioned structures using Strand7 and different types of analyses, which are discussed below.

3.3. Types of Analyses

Four types of analyses were performed using Strand7 to evaluate the performance of DFF, ACH and PERIH in different conditions. These analyses are linear static, natural frequency, spectral response, and steady-state heat.

3.3.1. Linear Static Analysis

Linear static analysis is a common solver in Strand7, which analyses the structure based on the following two key assumptions:

(1)   The response of the structure is linear.
(2)   The loading on the structure is static.

This implies that the structure's mechanical properties must follow Hooke's law. Moreover, the deformation of the structure must be significantly small and proportionate to its undeformed state [45]. The linear static solver is performed by considering the stiffness, nodal displacement, and force for each element in the discretised structure. Through an assembly process, the individual element matrices are then assembled to form the global matrix of the system (Equation (1)).

$$[K]\{d\} = \{F\} \tag{1}$$

The global matrix links the global nodal force vector, $\{F\}$, to the product of the global stiffness matrix, $[K]$, and unknown nodal displacement vectors, $\{d\}$. This enables finding the stresses, strains and reactions on the nodes and elements.

Linear static solver is a widely used solution to analyse the structures and was also used in this paper. However, the assumption of analysing the undeformed state and having a perfectly linear relationship between stress and strain is not always valid. This introduces another type of analysis called the non-linear static analysis, which is out of the scope of this paper due to its negligible difference from the linear static analysis.

3.3.2. Natural Frequency Analysis

The natural frequency of a structure is defined as the rate at which the structure vibrates naturally when disturbed. The vibration rate depends on the structure's stiffness, mass, and vibration mode.

This relationship can be formulated using Equation (2), where $[K]$ is the global stiffness matrix, $[M]$ is the global mass matrix, $\{x\}$ is the vibration mode vector, and ω is the natural frequency.

$$[K]\{x\} = \omega^2[M]\{x\} \tag{2}$$

The equation above shows that the natural frequency is directly proportional to the stiffness and inversely proportional to the mass. This can provide critical insights into controlling the behaviour of the structures. For example, increasing the mass leads to a decrease in the natural frequency of the structure. Therefore, damping is typically used in tall buildings to reduce the vibration due to the wind and seismic load.

The vibration mode, also called mode shape, is another critical factor in the natural frequency analysis, which is defined as the pattern of vibration the structure follows when excited [46]. Structures can have multiple mode shapes, and each mode shape is associated with a specific natural frequency [47].

In practice, the natural frequency analysis is used to obtain the natural frequencies and mode shapes, which can be used to find the relative displacement. In addition, the natural frequency can be used to check the frequency range of the structure in different conditions [47]. For example, natural frequency analysis is often used to check the frequency range of the structure against the external frequencies caused by the wind and seismic load. Having a similar structure and external frequency can reinforce the vibration, leading to the inconvenience of the occupants and potential failure of the structure.

The natural frequency solver is performed by considering the stiffness and mass matrices for each individual element in the discretised structure. These matrices are assembled through the assembly to form the global stiffness and mass matrices. The frequencies and the mode shapes are obtained by solving the eigenvalue problem, using the method of sub-space iteration [48].

3.3.3. Spectral Response Analysis

The spectral response analysis is used to analyse the behaviour of a structure during random dynamic loading, such as an earthquake. This analysis depends on the spectral curve of the earthquake specified by the standards and varies from one country to another. For example, the spectral curve of the earthquake in Australia is governed by AS 1170.4 [49].

The mass participation factor is another important concept during random dynamic loading, which can be obtained using spectral response analysis. The mass participation factor indicates the percentage of the structure mass moving in a particular mode. A high mass participation factor is desirable, and AS 1170.4 recommends having at least 90% of the structure's mass participate during dynamic loading. However, factors such as the significant difference between members' stiffness in the structure can reduce the mass participation factor.

According to Strand7 [50], the spectral response solver for seismic loading is performed by assembling the mass matrix for each element to find the vibration factors for each vibration mode obtained in the natural frequency analysis. This, combined with the defined spectral curves, enables finding the mass participation factor of each mode and the relative displacement of the structure.

3.3.4. Steady-State Heat Analysis

The steady state heat analysis can be used to calculate the distribution of temperature when the structure is in equilibrium. This analysis can be performed linearly and non-linearly, depending on the material properties. In the linear analysis, the temperature changes with time and the material properties do not depend on the temperature. On the

contrary, the non-linear analysis assumes the dependency between the temperature and material properties.

The steady-state heat analysis is governed by Equation (3), where [K] is the conductivity matrix, {F} the applied force vector, and {T} the vector of nodal temperatures. The nodal temperature, flux, and temperature gradients can be calculated using this equation.

$$[K]\{T\} = \{F\} \tag{3}$$

The steady state heat analysis is performed by assembling the conductivity matrices and the applied vectors obtained from the nodal temperatures and the coefficients of radiation and convection. This enables finding the unknown temperature at each node and calculating the heat flux and temperature gradients. Moreover, the node flux can be used to derive the total heat flow, *Q*, of the system (Equation (4)), which can provide insights into the energy cost and optimisation methods [51].

$$Q = \sum_{t=0}^{n} \sum_{nodes} NodeFlux.\Delta t \tag{4}$$

It is important to note that realistically, the temperature varies with time, and hence the transient heat analysis yields the most accurate result. However, due to various unknown parameters required by the transient solver and limited standards, this paper performed the steady-state heat analysis to get insights into the energy consumption of the structures.

3.4. Common Details of All Analyses

As mentioned in Section 3.3, four types of analyses were performed using Strand7 to evaluate the performance of each structure. This section aims to discuss the common details used in establishing these.

3.4.1. Standards

This paper used the Australian Standard (AS) as the main standard throughout the analyses; however, some references were also made to Eurocode 1. The specific standards used are summarised in Table 3.

Table 3. Standards used in the analyses.

Standards	Description
AS/NZS 1170.1 [52]	Permanent, imposed, and other actions
AS/NZS 1170.2 [53]	Wind actions
AS/NZS 1170.4 [49]	Earthquake loads
AS 3600 [54]	Design properties of material
AS/NZS 4859.1 [55]	Materials for thermal insulation
Eurocode 1 [56]	Actions on structures

3.4.2. Load Combinations

Structures are often subjected to different loads, such as dead (G), live (Q), and wind (W) loads. Load combinations can be used to ensure the safety of the structure under various loading conditions.

Two limit states are used to measure the load combinations of the structure. These limit states are the serviceability limit state (SLS) and the ultimate limit state (ULS). SLS is associated with the behaviour of the structure, such as vibration, while ULS focuses on the failure criteria. Based on AS/NZS 1170.1 and Eurocode 1, the following load combinations, shown in Table 4, were considered during the analyses.

Table 4. SLS and ULS load combinations used in the analyses.

Serviceability Limit State (SLS)		Ultimate Limit State (ULS)	
Load Combination	**Description**	**Load Combination**	**Description**
$1.35G$	Net destabilising	$0.9G + W$	Permanent and wind action
$1.2G + 1.5Q$	Permanent and imposed action	$1.35G + 1.5Q$	Permanent and imposed action
$G + 0.7Q + W$	Permanent, imposed and wind action	$1.35G + 1.05Q + 1.5W$	Permanent, imposed and wind action

3.4.3. Material Properties

Concrete and steel were used as the primary materials in this paper, in accordance with AS 3600 [54] and AS 4100 [57]. The material properties of concrete and steel are summarised in Tables 5 and 6, respectively.

Table 5. Structural and thermal properties of concrete.

Structural Properties	Value
Compressive strength (After 28 days)	32 MPa
Modulus of elasticity	3.1×10^7 kPa
Poisson's ratio	0.2
Density	2400 kg/m^3
Thermal Properties	**Value**
Thermal expansion	0.00001/C
Specific heat	880 J/kg/C
Conductivity	1.37 J/s/m/C

Table 6. Structural and thermal properties of steel.

Structural Properties	Value
Modulus of elasticity	2×10^8 kPa
Poisson's ratio	0.25
Density	7850 kg/m^3
Thermal Properties	**Value**
Thermal expansion	1.17×10^{-5}/C
Specific heat	465 J/kg/C
Conductivity	54 J/s/m/C

3.4.4. Boundary Conditions

As the structures are sitting on a rigid foundation, a rigid connection was used at the base. This was done by selecting all the nodes at the base and restraining in the X, Y and Z direction.

3.5. Idealisation

Various idealisations were made for DFF and PERIH to reduce the computational time, while keeping the accuracy within a reasonable range. These idealisations are discussed in the following sections.

3.5.1. Idealisations for DFF

The substructure of DFF was ignored during the modelling due to probable incompatibility between the types of elements. However, a similar effect to the foundation was created by fully fixing the node on the base of the cassette in all the directions, as illustrated in Figure 2.
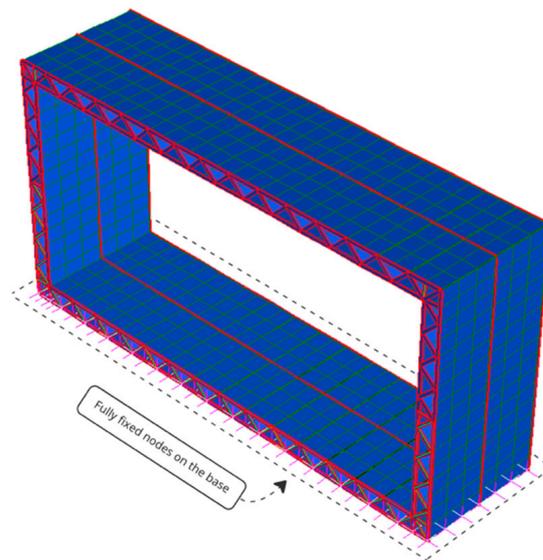
Figure 2. Fully fixed nodes on the base of the cassette to provide a foundation effect.

The original structure consisted of four cassettes. However, only one cassette was analysed due to the principle of superposition. Moreover, the rounded corners of the structure were also ignored because of their negligible effect on the behaviour of the structure.

3.5.2. Idealisations for PERIH

PERIH is a two-level residential house. However, the thermal analysis was performed only on one level, and the result was expanded to the other level using the principle of similarity.

4. Results

The behaviour of each structure was studied using different types of analyses, as specified in Section 3.3. Each analysis was selected to capture a unique application of FEM in the analysis of the 3D-printed structures. Figure 3 summarises the types of analysis performed on each structure.

Type of analysis	DFF	ACH	PERIH
Linear static	✔		✔
Natural frequency	✔	✔	
Spectral response	✔	✔	
Steady-state heat	✔		✔

Figure 3. Types of analyses performed on each structure.

4.1. Strand7 Results for DFF

4.1.1. Linear Static Analysis of DFF

The linear static solver was used to obtain the maximum deflection of the structure in the vertical and lateral directions. This was done by measuring the maximum nodal displacement of the structure in each of the load combinations specified in Section 3.4.2.

The vertical displacement of the structure was mainly influenced by the effect of the permanent (dead) and imposed (live) loads. Figure 4 illustrates the deformed shape of the structure, with a displacement scale of 10%. The maximum vertical displacement occurred in the mid-span of the structure, which is associated with the maximum moment of $M_{max} = \frac{WL^2}{8}$.
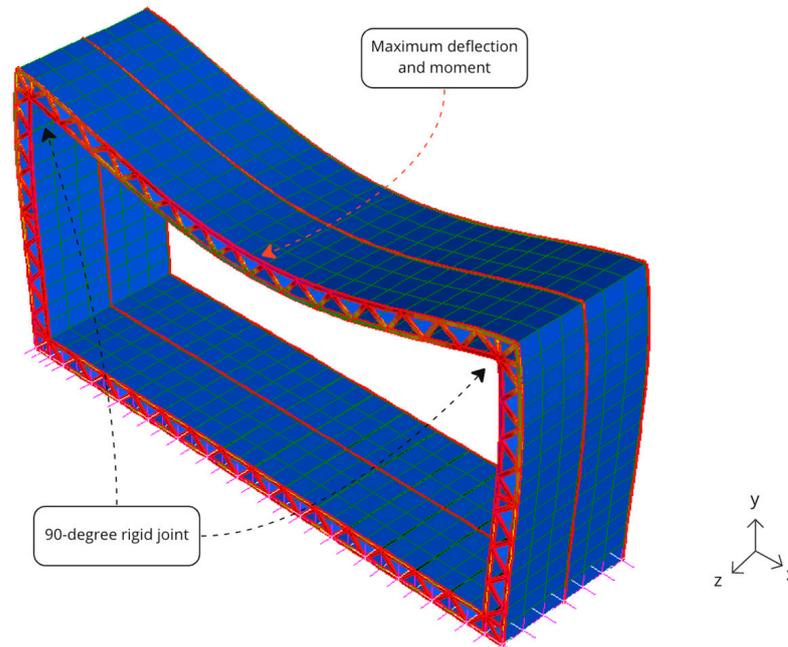
Figure 4. Deformed shape of DFF influenced by the dead and live loads.

To obtain the critical load combination, the maximum downward vertical displacement for each load combination was recorded and summarised in Figure 5.
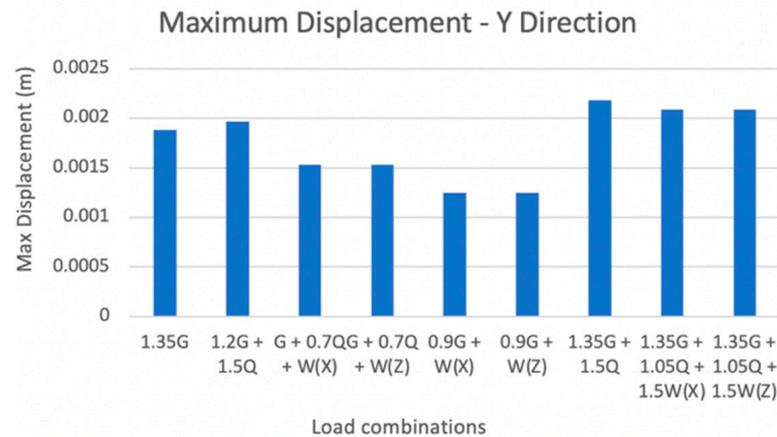
Figure 5. Maximum vertical displacement of DFF for each load combination.

It was observed that the maximum vertical displacement of the structure is equal to 0.00218 m and occurred under $1.35G + 1.5Q$. This load combination is considered the critical load combination of the structure and is associated with the ULS. Moreover,

this load combination is influenced by the dead and live load and hence, it is expected to occur in the mid-span of the structure due to the configuration similar to a simply supported beam.

The maximum lateral displacements were obtained by considering the wind effects in the lateral directions. Figure 6 represents the deformed shape of the structure due to the wind load in the X direction, with a displacement scale of 20%. The structure swayed due to the wind effect, with a 90-degree angle at the rigid joints. This caused tension and compression zones in each section, with the point of contraflexure in the middle of each section.
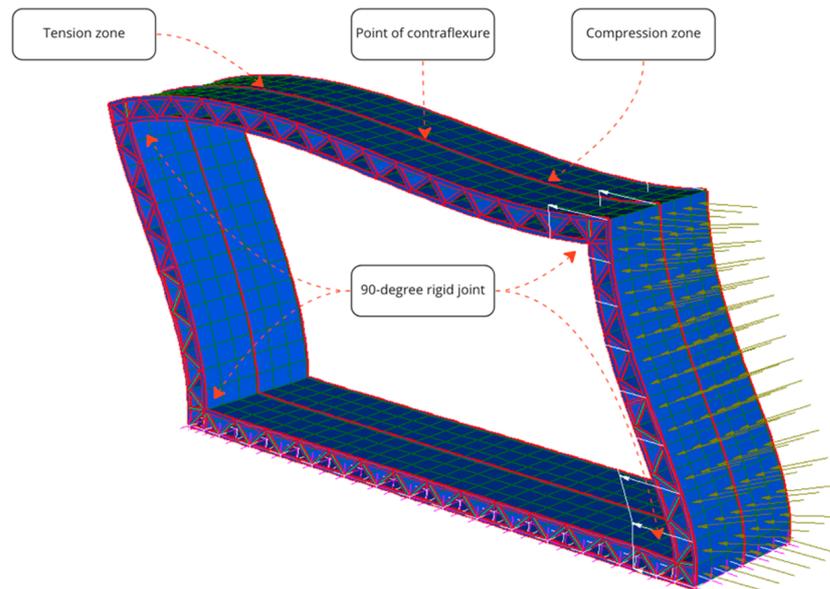
Figure 6. Deformed shape of DFF influenced by the wind load in the X direction.

Moreover, the maximum lateral displacements in the X direction were recorded and summarised in Figure 7.
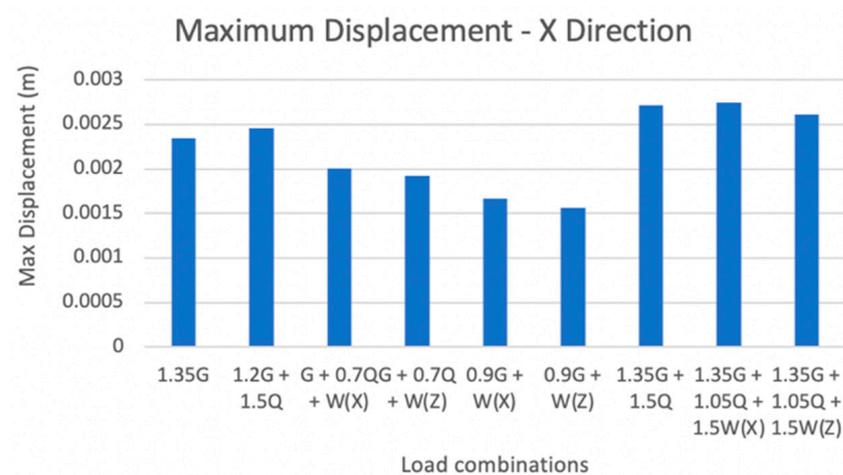
Figure 7. Maximum lateral displacement of DFF in the X direction for each load combination.

In this case, the critical load combination was $1.35G + 1.05Q + 1.5W(X)$, and is associated with the ULS, which resulted in a maximum nodal displacement of 0.00275 m in the X direction. Moreover, the load combination $1.35G + 1.5Q$ also resulted in a similar displacement, which indicates the significant influence of the dead and live loads applied to the structure.

The effect of lateral displacement in the Z direction was also studied by capturing the deformed shape of the structure, as shown in Figure 8. As mentioned earlier, the structure consists of four cassettes. Hence, the lateral displacement in the Z direction is less problematic in practice. This is because of the support provided by the other cassettes, leading to a significant reduction in the lateral displacement. Moreover, it is reasonable to analyse the deformed shape in the Z direction similar to a cantilever beam, with the maximum bending and displacement experienced at the bottom and top of the structure, respectively.
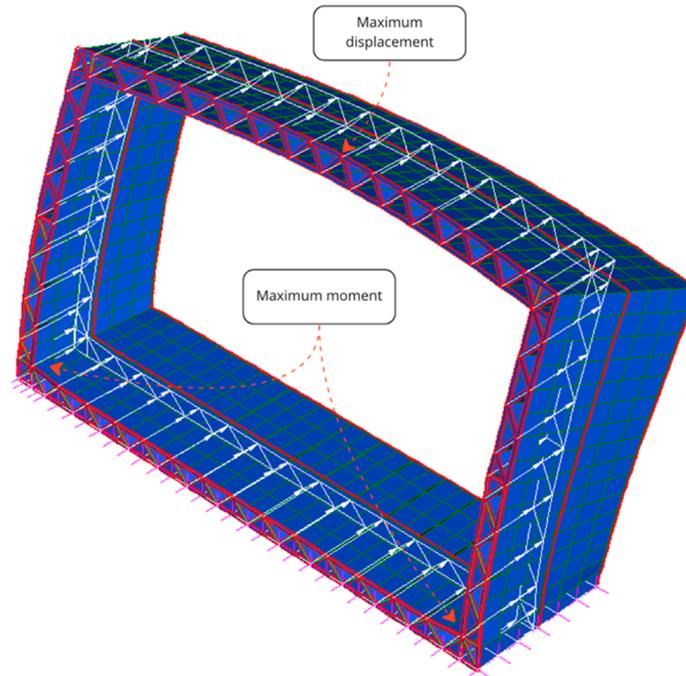
Figure 8. Deformed shape of DFF influenced by the wind load in the Z direction.

A maximum lateral displacement of 0.0000128 m was recorded in the Z direction. This displacement occurred under the critical load combination $1.35G + 1.05Q + 1.5W(Z)$, which is associated with the ULS. The values of the maximum lateral displacements in the Z direction are summarised in Figure 9.
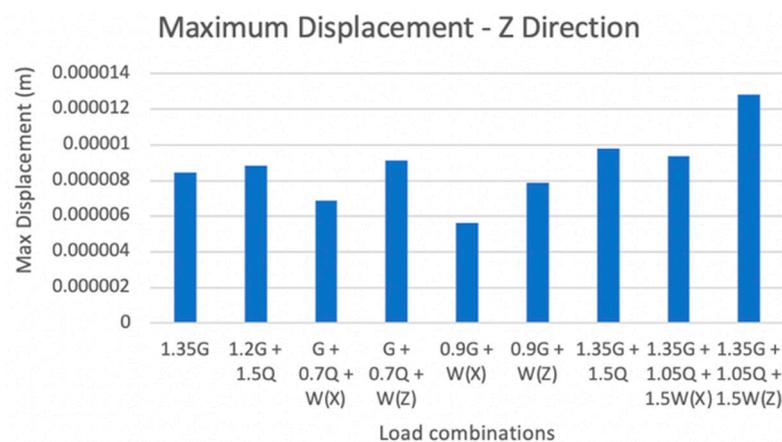
Figure 9. Maximum lateral displacement of DFF in the Z direction for each load combination.

4.1.2. Natural Frequency Analysis of DFF

The natural frequency solver was used to obtain the structure's different mode shapes and frequencies, and its relative displacement. This information is helpful in assessing the behaviour of the structure when excited by a frequency range, such as an earthquake or vibration due to human activities.

The nine modes were defined in Strand7, resulting in the associated natural frequencies shown in Table 7.

Table 7. Different modes and associated natural frequencies of the structure.

Mode	Value
Mode 1	8.21 Hz
Mode 2	15.14 Hz
Mode 3	21.66 Hz
Mode 4	33.86 Hz
Mode 5	41.65 Hz
Mode 6	44.65 Hz
Mode 7	57.83 Hz
Mode 8	66.29 Hz
Mode 9	68.14 Hz

Each mode caused the structure to deform in a certain way, as illustrated in Figure 10. It was observed that the structure experienced flexural, torsional, and flexural–torsional deformation at different frequencies.
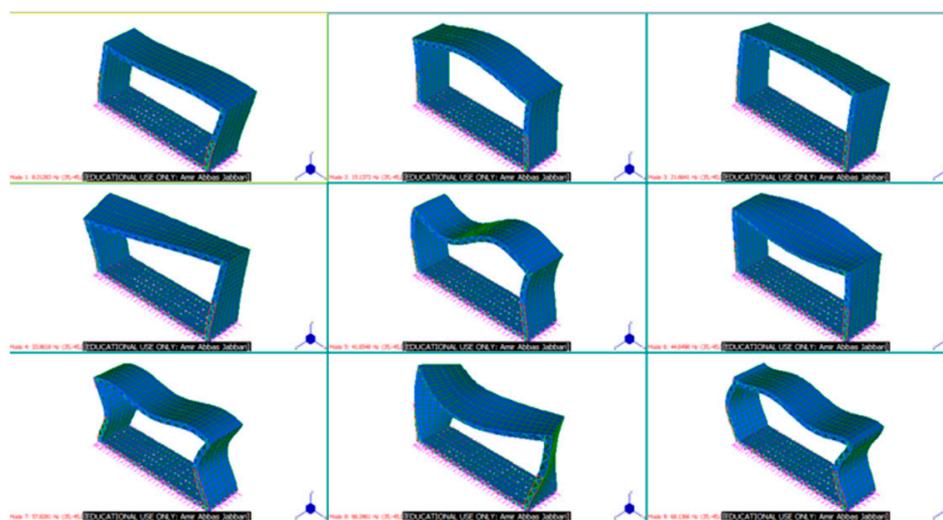
Figure 10. Deformed shape of the building associated with each mode.

The deformation of the structure was investigated by obtaining the maximum nodal displacement in the vertical and lateral directions for each of the modes, as summarised in Figure 11.

It was observed that mode 7 resulted in a maximum displacement of 0.017 m in the X direction. The displacement increased to 0.0272 m in the Y direction, caused by mode 6, and dropped to 0.0148 m in the Z direction in mode 4.

Maximum Displacements for Each Mode
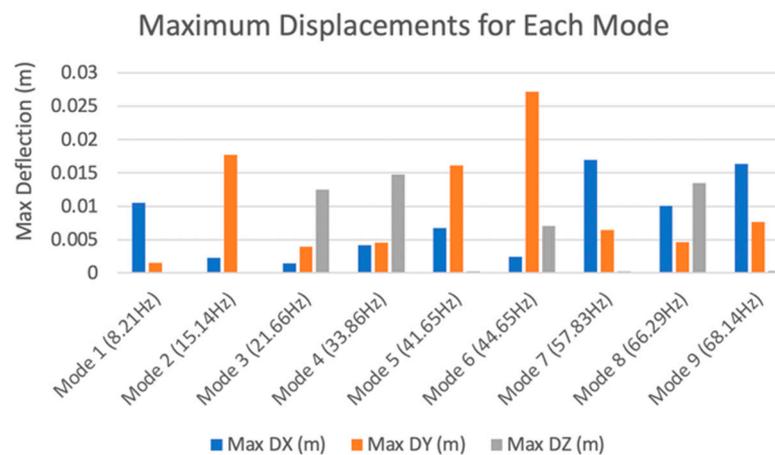
Figure 11. Maximum vertical and lateral nodal displacement for each mode.

4.1.3. Spectral Response Analysis of DFF

The spectral response solver was used to analyse the behaviour of the structure during random dynamic loading, such as an earthquake. This was done by obtaining the mass participation factor in each mode analysed, using the natural frequency solver.

Based on Figure 12, it was observed that the structure had a total mass participation of 31.01%, with mode 2 having the highest contribution of almost 25%. Moreover, modes 3, 4, 6, 7, and 8 had no contribution, which is not ideal during an earthquake. The reason for this is discussed in Section 5.

Mass Participation of Different Modes
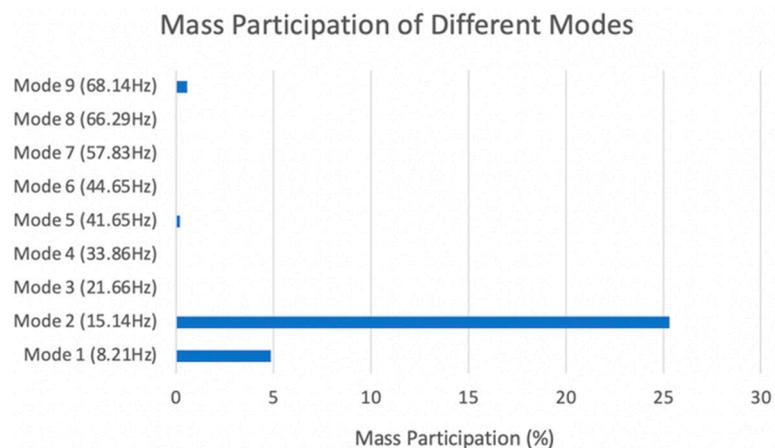
Figure 12. Mass participation of different modes.

The base shear and moment were also obtained to measure the effect of an earthquake on the base of the structure. This was done by using the method of square root of the sum of the squares (SRSS). The base shear and moment are shown in Table 8.

Table 8. Base shear and moment using SRSS.

Direction	Base Shear (kN)	Base Moment (kN.m)
X	427,000	1,030,000
Y	1,140,000	−786,000
Z	81,300	5,020,000

4.1.4. Steady-State Heat Analysis of DFF

A steady-state heat solver was used to investigate the temperature variation within the structure. This was done by defining the convection coefficient and convection ambient.

The convection coefficient is a material property which influences the rate of heat transfer, while the convection ambient is the temperature of the environment. Figure 13 represents the temperature distribution from the interior to the exterior of the structure.
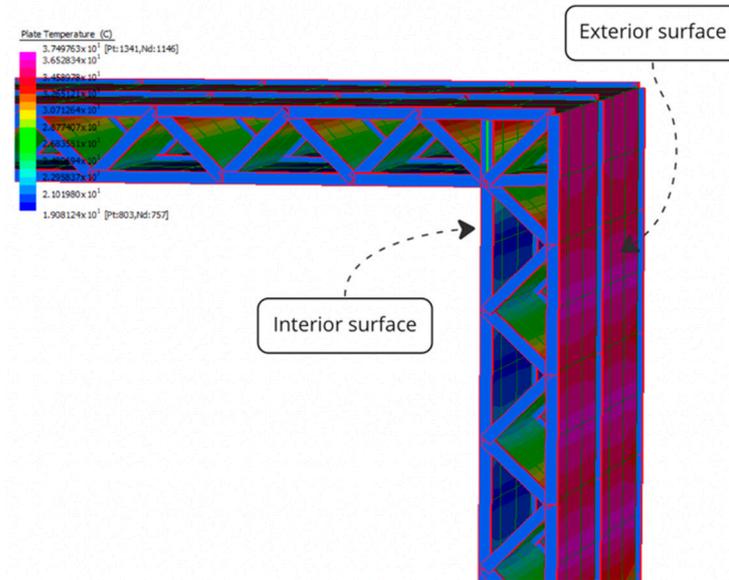

Figure 13. Distribution of temperature between the interior and exterior surface.

It was observed that the temperature decreased from the exterior surface to the interior surface. This was caused due to a higher exterior ambient temperature, defined based on the historical temperature in Dubai. The temperature variation experienced by the structure is captured in Figure 14, with 37.5 °C and 19.1 °C being the highest and lowest temperatures recorded, respectively.
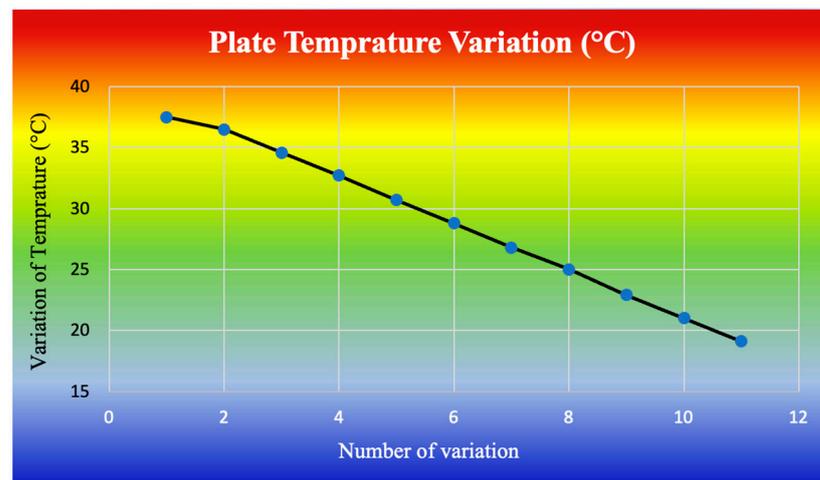
Figure 14. Temperature variation of the structure.

The total heat flux was obtained by summing the nodal flux within the boundary, resulting in a total flux of 64.4 J/s.

4.2. Strand7 Results for ACH

4.2.1. Natural Frequency Analysis of ACH

The natural frequency solver was used by defining nine modes, resulting in nine different natural frequencies summarised in Table 9.

Table 9. Different modes and associated natural frequencies of the structure.

Mode	Value
Mode 1	57.1 Hz
Mode 2	57.1 Hz
Mode 3	58.34 Hz
Mode 4	78.45 Hz
Mode 5	86.68 Hz
Mode 6	86.68 Hz
Mode 7	96.88 Hz
Mode 8	96.88 Hz
Mode 9	100.66 Hz

It was observed that some of the modes resulted in the same frequencies. This was due to the shape and geometry of the structure, resulting in the same frequencies. This behaviour and the deformed shape of the structure are shown in Figure 15.
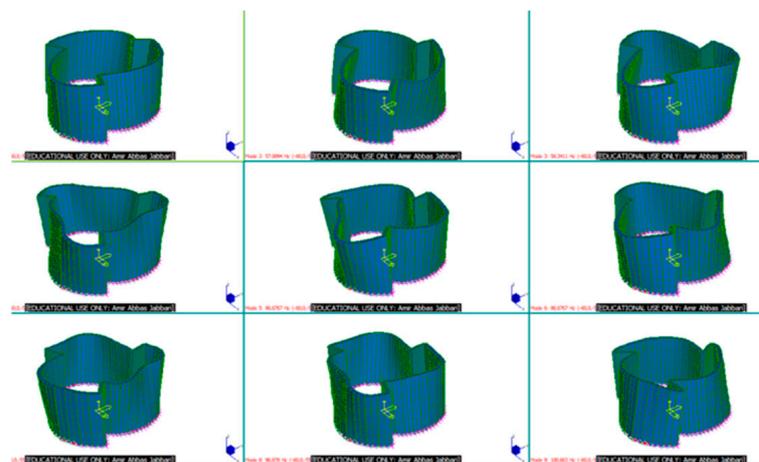
Figure 15. Deformed shape of the building associated with each mode.

In addition, the critical modes were found by obtaining the maximum nodal displacement in the vertical and lateral directions for each mode. These displacements are represented in Figure 16.
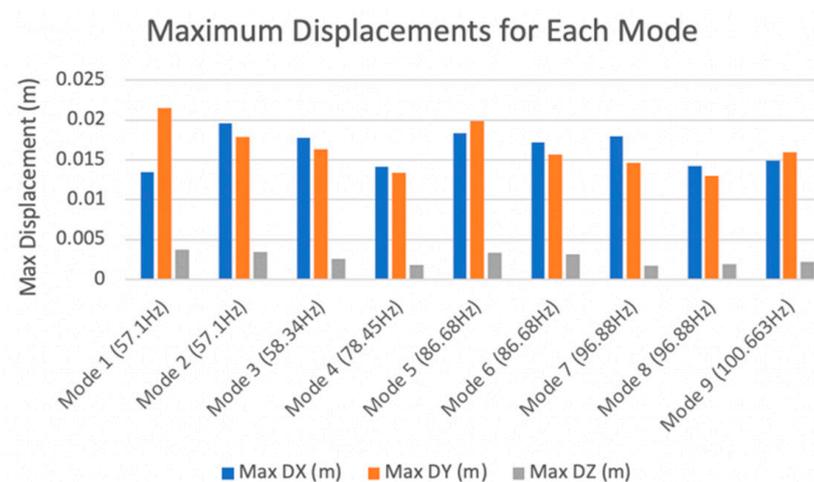

Figure 16. Maximum vertical and lateral nodal displacement for each mode.

Overall, it was observed that mode 1 was the critical mode, causing a maximum nodal displacement of 0.0215 m and 0.00372 m in the Y and Z directions, respectively. Moreover, the maximum displacement in the X direction was measured as 0.0196 m, resulting from mode 2.

4.2.2. Spectral Response Analysis of ACH

The mass participation factor of the structure was obtained using the spectral response solver and is shown in Figure 17.
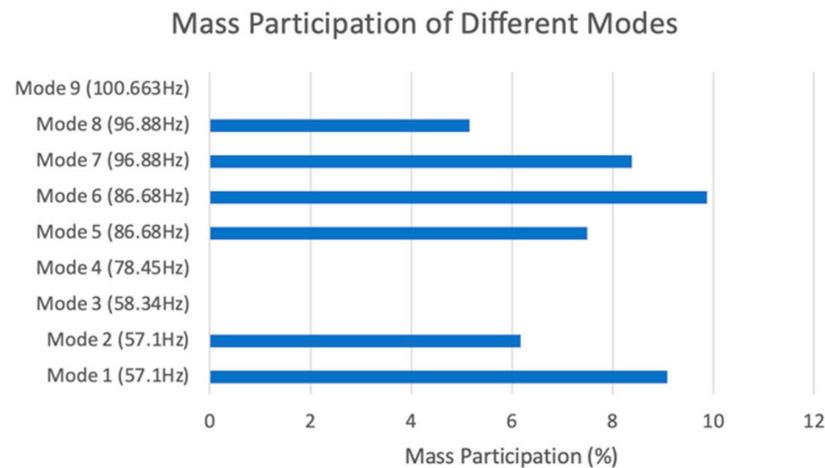

Figure 17. Mass participation of different modes.

The total mass participation of the structure was measured as 46.2%. Moreover, it was observed that ACH experienced a more distributed mass participation along all the modes, with mode 6 having the highest mass participation of 9.9%. In practice, having a uniform distribution among all the modes increases the effectiveness of the structure during the seismic load.

The base shear and moment were obtained by summing the nodal forces on the base of the structure, using the SRSS method. These values are summarised in Table 10.

Table 10. Base shear and moment using SRSS.

Direction	Base Shear (kN)	Base Moment (kN.m)
X	274,000	217,000
Y	277,000	−6900
Z	1,350,000	−19,000

4.3. Strand7 Results for PERIH

4.3.1. Linear Static Analysis of PERIH

Residential structures, including PERIH, are often impacted by floor vibration. This vibration can be caused by factors such as human activity and the type of floor system. Therefore, the linear static solver was used to mainly assess the behaviour of the level one floor system.

Figure 18 represents the deflected shape of the floor due to the dead and live loads, with a displacement scale of 10%. The floor experienced the largest deflection in the middle, depicted with the blue colour. This was due to the floor span of 15 m with no internal secondary beams. The deflection decreased along the boundaries due to the support provided by the walls.
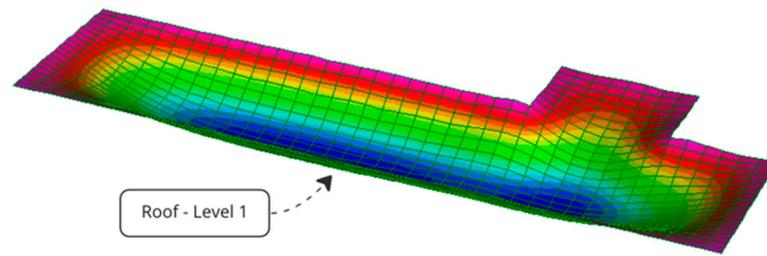
Figure 18. Deformed shape of the first floor influenced by the dead and live loads.

In addition, the maximum downward nodal displacement for each load combination was measured and is shown in Figure 19. It was seen that the floor could experience a maximum downward deflection of 0.0134 m under $1.35G + 1.5Q$. This is the critical load combination of the floor system and is associated with the ULS.
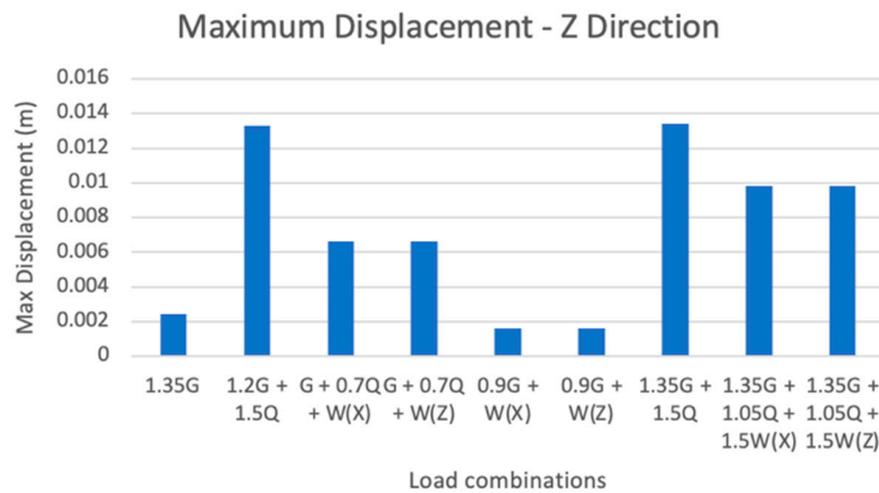

Figure 19. Maximum vertical displacement of the floor for each load combination.

4.3.2. Steady-State Heat Analysis of PERIH

A steady state heat solver was used to examine the temperature distribution through the walls. This was done by defining the convection coefficient and convection ambient. Figure 20 represents the temperature distribution from the interior to the exterior of the structure.
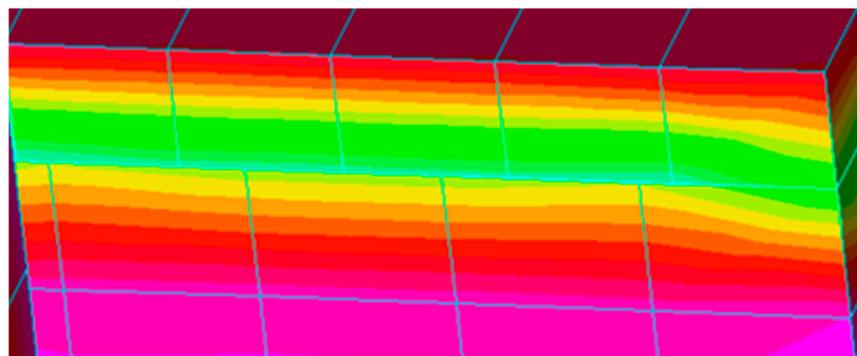

Figure 20. Distribution of temperature between the interior and exterior surface.

It was observed that the temperature increases by moving from the interior to the exterior surface. This was due to the lower ambient temperature defined in the analysis, which was obtained from the historical average temperature in Germany. The temperate

variation is shown in Figure 21 using a gradient, with 17.7 °C and 0.5 °C being the highest and lowest temperatures recorded, respectively.
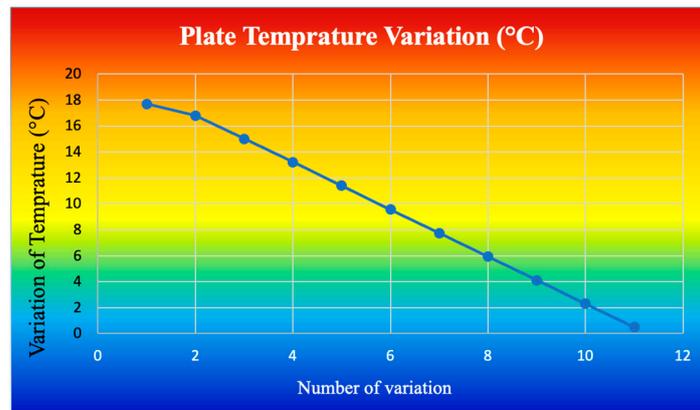

Figure 21. Temperature variation of the structure.

In addition, a total heat flux of 75.1 J/s was recorded for the wall boundaries, by summing the nodal flux within that region.

5. Discussion

Strand7 was used to investigate three 3D-printed structures, by performing four types of analyses. Each analysis aimed to assess the performance and examine the application of FEM in the analysis of the 3D-printed structures as a future direction in the Construction Industry 4.0. However, the validation of results is required to assess the reliability of FEM in analysing 3D-printed structures. It is also important to obtain the source of errors and ways to address them.

5.1. Validation of the Results

The validation process was done by comparing the results obtained in Section 4 with the available standards. Table 11 summarises the available standards for each type of analysis performed.

Table 11. Validation of the analyses, in accordance with the available standards.

Analysis	Main Objective	Relevant Standards
Linear Static	Vertical and lateral displacement	AS 3600 ACI
Natural Frequency	Structural vibration	AS 3600 EN 1991-1 [58]
Spectral Response	Mass participation factor	EN 1998-1 [59]

5.1.1. Validation of Linear Static Results

The linear static analysis was performed on DFF and PERIH to find the structure's critical load combination and associated maximum vertical and lateral displacement. AS 3600 and ACI were used to check the maximum permissible vertical and lateral displacements, respectively.

According to Table 2.4.2 of AS 3600-2001, it is recommended to have a total vertical deflection limit of L/250 for all structural members. Since DFF has a span of 8.1 m, the maximum recommended vertical deflection according to AS 3600 is 0.032 m. Figure 22 compares DFF's maximum vertical displacement for each load combination with the suggested deflection limit.

Maximum Displacement - Y Direction
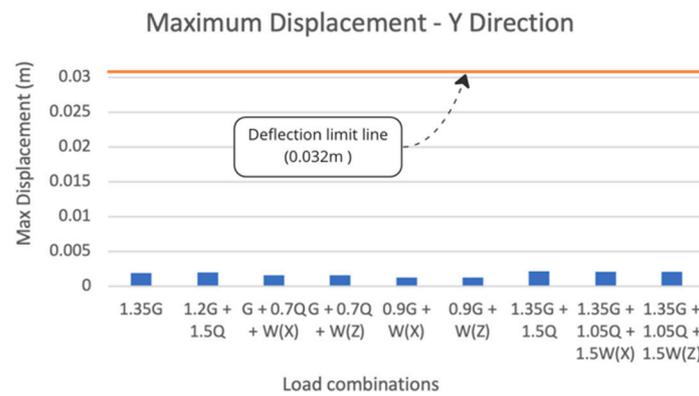
Figure 22. Deflection limit and the maximum vertical deflection for each load combination for DFF.

All the deflections were observed to comply with the deflection limit specified by AS 3600, with an average difference of approximately 174%.

Similarly, a total floor deflection limit of 0.06 m was obtained for PERIH, based on a floor span of 15 m. As shown in Figure 23, the maximum floor deflection in all the load combinations is below the suggested limit by approximately 127%.

Maximum Displacement - Z Direction
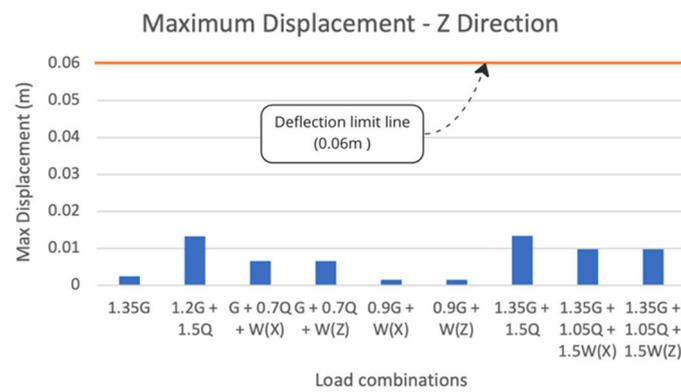
Figure 23. Deflection limit and the maximum vertical deflection for each load combination for PERIH.

For the lateral deflection, ACI recommends a total limit of H/500 for all structural members. This equates to a lateral deflection limit of 0.0084 m for DFF, based on the height of 4.2 m used in each cassette. Figure 24 compares the maximum lateral displacement with the suggested limit.

Maximum Displacement - X Direction
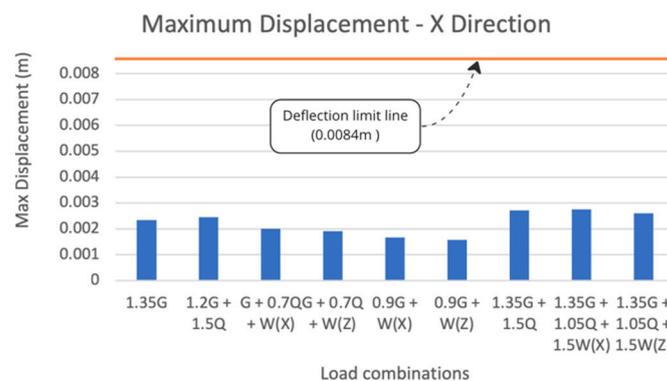
Figure 24. Deflection limit and the maximum lateral deflection for each load combination for DFF.

It was observed that the maximum lateral deflection of the structure complies with the ACI limit, with an average difference of 101.3%.

Overall, DFF and PERIH had a maximum displacement below the recommended limits. This indicates the compliance with the standards ULS and SLS.

5.1.2. Validation of Natural Frequency Results

The natural frequency analysis was performed on DFF and ACH to obtain the vibration of the structure and relative deflection for each mode. AS 3600 was used to compare the maximum deflection for each mode, with the deflection limit and EN 1991-1 to examine the frequency of the structure.

Figure 25 shows the maximum vertical deflection that occurred by each mode against the suggested total limit specified by AS 3600.
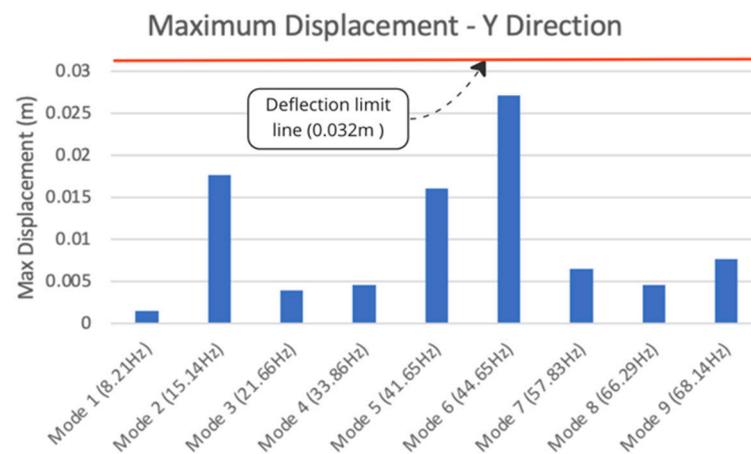

Figure 25. Deflection limit and the maximum vertical deflection for each frequency mode.

It was observed that the deflection of the structure complies with the standard, even at higher frequencies. Moreover, a minimal gap between the deflection and limit was observed caused by the dead load and wind load in the Z direction, influencing mode 6 $0.9G + W(Z)$. This is important to ensure the stability of the structure during dynamic loadings, such as seismic loads.

EN 1991-1-1-1 recommends a minimum natural frequency of 8.4 Hz for the structure. The minimum natural frequency obtained for ACH was 54.1 Hz, which satisfies the limit. However, DFF had a minimum natural frequency of 8.21 Hz, slightly below the suggested 8.4 Hz limit, by 2.3%. This is an acceptable tolerance and would not affect the performance of the structure [60]. However, the reason for this difference can be justified using the formula for natural frequency, as shown by Equation (5).

$$f = \frac{17.8}{\sqrt{\delta}} \approx \frac{18}{\sqrt{\delta}} \tag{5}$$

The maximum deflection (δ) is dependent on the gross second moment of area, loading and mesh quality, which were influenced by the idealisations made in Section 3.5.1. This affected the maximum deflection and resulted in a slightly different natural frequency.

5.1.3. Validation of Spectral Response Results

The spectral response analysis was performed on DFF and ACH, to investigate the performance under seismic load. This was done by obtaining the mass participation factor and calculating the base shear and moment.

There are no standards regarding the permissible base shear and moment, and the obtained results were only informative data that can be used to ensure the stability of the base of the structure.

The mass participation factor was compared to EN 1998-1. Based on this standard, the structure is recommended to have a total mass participation of at least 90%. Figure 26

shows the suggested limit against the mass participation factors obtained for DFF and ACH.
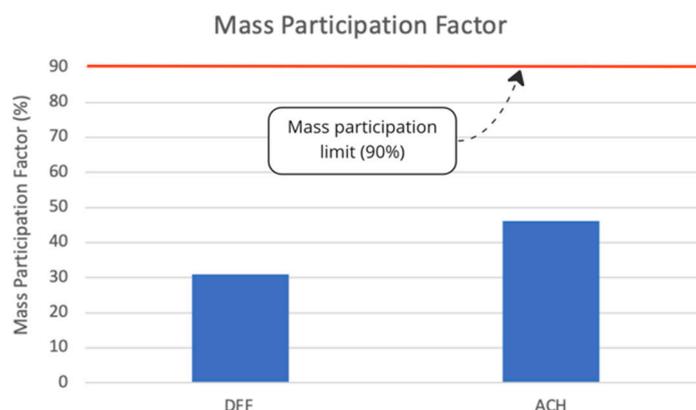

Figure 26. Mass participation factor of DFF and ACH against the suggested limit.

Both structures failed to comply with this standard. The main reason for this is the stiffness of the elements. Both structures used concrete as the main material, which has a high stiffness. As a result, the mass participation of the structure was governed by the stiffness of the concrete members, resulting in a less dynamic response and a lower mass participation factor. Another reason is related to the standards. The spectral response analysis depends on the spectral curve of the earthquake specified by the standards, and varies from country to country. In both analyses, AS 1170.4 was used, resulting in an underestimation of the results due to limited earthquakes in Australia. This could have been adjusted by accessing UAE's and Germany's spectral curves, which this paper could not access.

5.1.4. Validation of Steady-State Heat Results

The steady-state heat analysis was performed on DFF and PERIH to investigate the temperature variation within the interior and exterior surfaces. There are no standards governing the required temperature variation; however, this information can be used to approximate the energy cost of the structure, using the total heat flux.

The total flux of DFF was obtained as 64.4 J/s, equivalent to 64.4 W. Assuming constant heat flux, the total flux for one week can be calculated by multiplying the total flux by 0.168. This results in a total flux of 10.8 kWh per week. Assuming an energy rate of AUD 0.28/kWh, this equates to AUD 3.02 per week to heat the corner shown in Figure 13.

Similarly, PERIH had a total flux of 75.1 J/s or 75.1 W. Following the above procedure, it results in a weekly energy cost of AUD 3.53 to heat the corner represented in Figure 20.

5.2. Errors and Improvements

Reasonable effort was made in this paper to minimise the errors. These errors are mainly due to meshing, idealisations, and standards.

Meshing can influence the accuracy of the results; however, having a fine mesh can significantly increase the computational time and cost of the analysis. This was addressed by introducing finer mesh only in the areas of interest, such as corners and mid-spans.

DFF and PERIH were idealised, as discussed in Section 3.5. This was done to run the analysis without modelling the fine details that have negligible influence on the overall performance. The errors due to idealisation are insignificant in the performed analysis and were addressed by alternative approaches covered in Section 3.5.

Standards had the most effect in this paper, as they govern the analysis and vary for each country. Errors caused by the standards did not lead to incorrect results or discussion; instead, they reflected the results based on the country of the standard, mainly Australia. This could have been improved by using the relevant standards for UAE, Russia, and Germany.

5.3. Recommendation for Future Research

This paper aimed to analyse the critical performance of 3D-printed structures. However, future research is required to improve the implementation of 3D printing in the construction industry.

Currently, manual work is required to place the reinforcing bars between the concrete layers. However, there is a potential to replace the reinforcing bars by introducing a stronger concrete mix, such as ultra-high-performance concrete (UHPC).

Quality control is another key area that needs to be investigated to ensure the consistency of the concrete paste. This can be further enhanced by the application of artificial intelligence (AI), machine learning (ML), and image processing.

It is also recommended to conduct further research on the legislative requirements of 3D printing in construction. The framework provided by the Construction Industry 4.0 and discussed in Section 2.1 can be used as a guideline for undertaking this research.

6. Conclusions

The 3D printing technology is a promising AM method in construction. It is automated, flexible, innovative, and sustainable. Moreover, it aligns with SDGs, making it an attractive solution in the Construction Industry 4.0. Given the future potential of AM, this paper performed a detailed analysis of 3D-printed structures.

Three 3D-printed structures were analysed based on FEM, to examine the performance of the structures and the application of FEM in assessing 3D-printed structures. Four analyses were performed, including linear static, natural frequency, spectral response, and steady-state heat. The obtained results provided an overview of the behaviour of each structure. However, validation was required to ensure the results' accuracy and the structures' compliance with the relevant standards, which was done by comparing the results with the requirements of the standards. It was seen that FEM reasonably analysed the 3D-printed structures, and most of the results complied with the relevant standards. This highlights the application of AM and FEM as the future direction in the Construction Industry 4.0.

References

1. Kumar, S.; Prasad, R. *Basic Principles of Additive Manufacturing: Different Additive Manufacturing Technologies*; Woodhead Publishing: Sawston, UK, 2021; pp. 17–35.
2. Maskuriy, R.; Selamat, A.; Ali, K.; Maresova, P.; Krejcar, O. Industry 4.0 for the Construction Industry—How Ready Is the Industry? *Appl. Sci.* **2019**, *9*, 2819. [CrossRef]
3. Pradhan, P.; Costa, L.; Rybski, D.; Lucht, W.; Kropp, J. A Systematic Study of Sustainable Development Goal (SDG) Interactions. *Earth's Future* **2017**, *5*, 1169–1179. [CrossRef]
4. Google Trends. 3D Printing in Construction. 2022. Available online: https://trends.google.com/trends/explore?date=all&q= 3D%20printing%20in%20construction (accessed on 16 April 2022).
5. Macneal, R.; Harder, R. A proposed standard set of problems to test finite element accuracy. *Finite Elem. Anal. Des.* **1985**, *1*, 3–20. [CrossRef]

6. Abbot, D.; Kallon, D.; Anghel, C.; Dube, P. Finite Element Analysis of 3D Printed Model viaCompression Tests. *Procedia Manuf.* **2019**, *35*, 164–173. [CrossRef]

7. Hossain, M.; Nadeem, A. Towards Digitizing the Construction Industry: State of the Art of Construction 4.0. *Proc. Int. Struct. Eng. Constr.* **2019**, *6*, 3–7. [CrossRef]

8. Li, J.; Yang, H.A. Research on Development of Construction Industrialization Based on BIM Technology under the Background of Industry 4.0. *MATEC Web Conf.* **2017**, *100*, 02046. [CrossRef]

9. Oesterreich, T.D.; Teuteberg, F. Understanding the Implications of Digitisation and Automation in The Context of Industry 4.0: A Triangulation Approach and Elements of a Research Agenda for The Construction Industry. *Comput. Ind.* **2016**, *83*, 121–139. [CrossRef]

10. Chen, Q.; García de Soto, B.; Adey, B.T. Construction Automation: Research Areas, Industry Concerns and Suggestions for Advancement. *Autom. Constr.* **2018**, *94*, 22–38. [CrossRef]

11. Dallasega, P.; Rauch, E.; Linder, C. Industry 4.0 As an Enabler of Proximity for Construction Supply Chains: A Systematic Literature Review. *Comput. Ind.* **2018**, *99*, 205–225. [CrossRef]

12. Wright, S. Why would a Construction Business have a Document Management System? *Credit. Control* **2013**, *34*, 70.

13. Global Industry 4.0 Survey. Engineering and Construction Key Findings. 2016. Available online: https://www.pwc.nl/nl/assets/documents/industry-4-0-engineering-and-construction-key-findings.pdf (accessed on 5 April 2022).

14. Keating, S.J.; Leland, J.C.; Cai, L.; Oxman, N. Toward Site-Specific and Self-Sufficient Robotic Fabrication on Architectural Scales. *Sci. Robot.* **2017**, *2*, eaam8986. [CrossRef] [PubMed]

15. Woodhead, R.; Stephenson, P.; Morrey, D. Digital Construction: From Point Solutions to Iot Ecosystem. *Autom. Constr.* **2018**, *93*, 35–46. [CrossRef]

16. Streule, T.; Miserini, N.; Bartlomé, O.; Klippel, M.; de Soto, B.G. Implementation of Scrum in the Construction Industry. *Procedia Eng.* **2016**, *164*, 269–276. [CrossRef]

17. World Economic Forum. Shaping the Future of Construction: A Breakthrough in Mindset and Technology. 2016. Available online: http://www3.weforum.org/docs/WEF_Shaping_the_Future_of_Construction_full_report__.pdf (accessed on 5 April 2022).

18. Hager, I.; Golonka, A.; Putanowicz, R. 3D Printing of Buildings and Building Components as the Future of Sustainable Construction? *Procedia Eng.* **2016**, *151*, 292–299. [CrossRef]

19. Davtalab, O.; Kazemian, A.; Khoshnevis, B. Perspectives on a BIM-integrated software platform for robotic construction through Contour Crafting. *Autom. Constr.* **2018**, *89*, 13–23. [CrossRef]

20. Volk, R.; Stengel, J.; Schultmann, F. Building Information Modeling (BIM) for existing buildings-Literature review and future needs. *Autom. Constr.* **2014**, *38*, 109–127. [CrossRef]

21. El-Sayegh, S.; Romdhane, L.; Manjikian, S. A critical review of 3D printing in construction: Benefits, challenges, and risks. *Arch. Civ. Mech. Eng.* **2020**, *20*, 8–12. [CrossRef]

22. Kietzmann, J.; Pitt, L.; Berthon, P. Disruptions, decisions, and destinations: Enter the age of 3-D printing and additive manufacturing. *IEEE Eng. Manag. Rev.* **2017**, *45*, 98–104. [CrossRef]

23. Sanjayan, J.G.; Nazari, A.; Nematollahi, B. *3D Concrete Printing Technology: Construction and Building Applications*; Butterworth-Heinemann: England, UK, 2019.

24. Brenken, B.; Barocio, E.; Favaloro, A.; Kunc, V.; Pipes, R.B. Fused filament fabrication of fiber-reinforced polymers: A review. *Addit. Manuf.* **2018**, *21*, 16. [CrossRef]

25. Guenther, D. 3D printing–The state of the technology and the future of this process. *Detail–Technol.* **2015**, 596–600. [CrossRef]

26. Tahmasebinia, F.; Sepasgozar, S.M.E.; Shirowzhan, S.; Niemela, M.; Tripp, A.; Nagabhyrava, S.; Mansuri, K.K.Z.; Alonso-Marroquin, F. Criteria development for sustainable construction manufacturing in Construction Industry 4.0. *Constr. Innov.* **2020**, *20*, 379–400. [CrossRef]

27. Feng, P.; Meng, X.; Zhang, H. Mechanical behavior of FRP sheets reinforced 3D Elements printed with cementitious materials. *Compos. Struct.* **2015**, *134*, 331–342. [CrossRef]

28. Buswell, R.A.; Soar, R.C.; Gibb, A.G.F.; Thorpe, A. Freeform Construction: Mega scale rapid manufacturing for construction. *Autom. Constr.* **2007**, *16*, 224–231. [CrossRef]

29. World Economic Forum. Winsun: Demonstrating the Viability of 3D Printing at the Construction Scale. 2016. Available online: https://futureofconstruction.org/case/winsun/ (accessed on 15 December 2019).

30. Wu, P.; Wang, J.; Wang, X. A critical review of the use of 3-D printing in the construction industry. *Autom. Constr.* **2016**, *68*, 21–31. [CrossRef]

31. García-Alvarado, R.; Moroni-Orellana, G.; Banda-Pérez, P. Architectural Evaluation of 3D Printed Buildings. *Buildings* **2021**, *11*, 254. [CrossRef]

32. Delgado Camacho, D.; Clayton, P.; O'Brien, W.J.; Seepersad, C.; Juenger, M.; Ferron, R.; Salamone, S. Applications of additive manufacturing in the construction industry–A forward-looking review. *Autom. Constr.* **2018**, *89*, 110–119. [CrossRef]

33. Ghaffar, S.H.; Corker, J.; Fan, M. Additive manufacturing technology and its implementation in construction as an eco-innovative solution. *Autom. Constr.* **2018**, *93*, 1–11. [CrossRef]

34. Hoek, M. Why 3D Printing is Key to Sustainable Business–Association of MBAs. Association of MBAs. Available online: https://www.associationofmbas.com/why-3d-printing-is-key-to-sustainable-business/ (accessed on 18 November 2022).

35. Labonnote, N.; Rønnquist, A.; Manum, B.; Rüther, P. Additive construction: State-of-the art, challenges and opportunities. *Autom. Constr.* **2016**, *72*, 347–366. [CrossRef]

36. Lim, S.; Buswell, R.A.; Le, T.T.; Austin, S.A.; Gibb, A.G.F.; Thorpe, T. Developments in construction-scale additive manufacturing processes. *Autom. Constr.* **2012**, *21*, 262–268. [CrossRef]

37. Sai Sandeep, U.; Muralidhara Rao, T. A Review on 3D Printing of Concrete-The Future of Sustainable Construction. *I-Manag. J. Civ. Eng.* **2017**, *7*, 49. [CrossRef]

38. Perkins, I.; Skitmore, M. Three-dimensional printing in the construction industry: A review. *Int. J. Constr. Manag.* **2015**, *15*, 1–9. [CrossRef]

39. Paul, S.C.; Tay, Y.W.D.; Panda, B.; Tan, M.J. Fresh and hardened properties of 3D printable cementitious materials for building and construction. *Arch. Civ. Mech. Eng.* **2018**, *18*, 311–319. [CrossRef]

40. Wolfs, R.J.M.; Bos, F.P.; Salet, T.A.M. Early age mechanical behaviour of 3D printed concrete: Numerical modelling and experimental testing. *Cem. Concr. Res.* **2018**, *106*, 103–116. [CrossRef]

41. Aragón, A.M.; Simone, A. The Discontinuity-Enriched Finite Element Method. *Int. Numer. Methods Eng.* **2017**, *112*, 1589–1613. [CrossRef]

42. Strand7-Overview. Strand7-Finite Element Analysis. Available online: https://www.strand7.com/html/brochure.htm (accessed on 20 November 2022).

43. Sakin, M.; Kiroglu, Y.C. 3D Printing of Buildings: Construction of the Sustainable Houses of The Future by BIM. *Energy Procedia* **2017**, *134*, 702–711. [CrossRef]

44. Madeleine, P. What Do We Know About the First 3D-Printed House Inaugurated in Germany?-3Dnatives. 3Dnatives. 5 August 2021. Available online: https://www.3dnatives.com/en/insights-into-germanys-first-3d-printed-house-050820214/#! (accessed on 24 November 2022).

45. Hughes, T.J.R. *The Finite Element Method: Linear Static and Dynamic Finite Element Analysis*; Dover Publications: Newburyport, MA, USA, 2012.

46. Braun, S.; Ewins, D.; Rao, S.; Leissa, A. Encyclopedia of Vibration: Volumes 1, 2, and 3. *Appl. Mech. Rev.* **2002**, *55*, B45. [CrossRef]

47. Goremikins, V.; Rocens, K.; Serdjuks, D.; Gaile, L. Experimental Determination of Natural Frequencies of Prestressed Suspension Bridge Model. *Constr. Sci.* **2013**, *14*, 32. [CrossRef]

48. Strand7 Solvers-Natural Frequency. Strand7-Finite Element Analysis. Available online: https://www.strand7.com/html/naturalfrequency/ (accessed on 16 November 2022).

49. *AS 1170.4*; Structural Design Actions, Part 4: Earthquake actions in Australia. Standards Australia: Sydney, Australia, 2007.

50. Strand7 Solvers-Spectral Response. Strand7-Finite Element Analysis. Available online: https://www.strand7.com/html/spectralresponse/ (accessed on 16 November 2022).

51. Strand7 Solvers-Heat. Strand7-Finite Element Analysis. Available online: https://www.strand7.com/html/steadystateheat/ (accessed on 21 November 2022).

52. *AS/NZS 1170.1*; Structural Design Actions—Permanent, Imposed and Other Actions. Standards Australia: Sydney, Australia, 2002.

53. *AS/NZS 1170.2*; Structural Design Actions Wind actions. Standards Australia: Sydney, Australia, 2021.

54. *AS 3600.3*; Concrete Structures. Standards Australia: Sydney, Australia, 2018.

55. *AS/NZS 4859.1*; Materials for the Thermal Insulation of Buildings—General Criteria and Technical Provisions. Standards Australia: Sydney, Australia, 2002.

56. *EN 1991*; Actions on Structures. Standards Australia: Sydney, Australia, 2002.

57. *AS 4100*; Steel Structures. Standards Australia: Sydney, Australia, 2020.

58. *EN 1991-1*; General Actions—Densities, Self-Weight, Imposed Loads for Buildings. Standards Australia: Sydney, Australia, 2002.

59. *EN 1998-1*; General Rules, Seismic Actions and Rules for Buildings. Standards Australia: Sydney, Australia, 2004.

60. Daniela, S. Re: In Finite Element Analysis Verification and Validation with Field Tests, Universally What Is the Expected Percentage Fea Should Meet? 2014. Available online: https://www.researchgate.net/post/In_finite_element_analysis_verification_and_validation_with_field_tests_universally_what_is_the_expected_percentage_FEA_should_meet/53fc5da6d039b129198b457c/citation/download (accessed on 17 November 2022).